Scripta Materialia 120 (2016) 19–22

Contents lists available at ScienceDirect

Scripta Materialia

journal homepage: www.elsevier.com/locate/scriptamat

Regular Article

In situ observations of Berkovich indentation induced phase transitions in crystalline silicon films

Yvonne B. Gerbig [a,b,*], Chris A. Michaels [a], Robert F. Cook [a]

[a] Material Measurement Laboratory, National Institute of Standards and Technology, Gaithersburg, MD 20899, USA
[b] School of Engineering & Applied Science, The George Washington University, Washington, DC 20052, USA

ARTICLE INFO

Article history:
Received 1 March 2016
Received in revised form 4 April 2016
Accepted 5 April 2016
Available online 19 April 2016

Keywords:
Raman spectroscopy
Silicon
Phase transitions
Nanoindentation

ABSTRACT

The pressure induced phase transitions of crystalline Si films were studied *in situ* under a Berkovich probe using a Raman spectroscopy-enhanced instrumented indentation technique. The observations suggested strain and time as important parameters in the nucleation and growth of high-pressure phases and, in contrast to earlier reports, indicate that pressure release is not a precondition for transformation to high pressure phases.

At atmospheric pressure, silicon (Si) has a diamond cubic (dc) structure. High pressure experiments in diamond anvil cell (DAC) tests indicate that under nearly hydrostatic conditions a phase transition from semiconducting dc to the metallic β-tin structure is initiated above a pressure threshold [1]. On further increase of pressure, tetragonal β-tin transforms into a phase with simple hexagonal structure (sh) via an orthorhombic phase (Imma). This phase transition sequence is reversible on slow decompression [1]. On further pressure release, β-tin does not recover to the dc phase: Other denser phases are formed, initially rhombohedral r8 which eventually transforms to cubic bc8 [1]. A significant difference between DAC tests and indentation experiments is the magnitude of the superposed deviatoric stress (and resulting shear strain) generated during indentation [2], especially when using acute indenter probes [3]. Theoretical and experimental studies indicate that the presence of shear strain may facilitate phase transitions, decrease transition pressures, and even change transition mechanisms in Si [4–7]. Unfortunately, access to the mechanically deformed region underneath the indenter probe is limited in conventional indentation instruments, allowing *in situ* observations of structural changes often only via indirect means. For example, *in situ* conductivity measurements during indentations on Si using acute, pyramidal probes (Vickers, Knoop, Berkovich) showed a decrease in resistance during loading, indicative of a transition to a more conductive phase [8–11]. However, due to a lack of capabilities for *in situ* structural characterization, the cause of the change in conductivity was not unambiguously identified and different mechanisms were considered: transition to β-tin (similar to DAC tests) [3] or amorphization [9,12–14]. Conclusions regarding the indentation-induced phase transformations were often based on analysis of the force–displacement data (the indentation curve), linking discontinuities in the curves with structural changes expected to occur based on DAC studies [3]. Based on such *ex situ* correlations, a possible transformation from β-tin to r8 was recently suggested to occur during cyclic indentation loading with a Berkovich probe [15]. Despite the progress, the indentation-induced phase transformation of Si using pyramidal probes is not fully understood. The study here focuses on the analysis of the phase transformation processes occurring during indentation of Si with a Berkovich probe by employing a newly developed technique that combines *in situ* Raman spectroscopy and instrumented indentation testing.

The contact region between a crystalline Si thin film and a Berkovich probe was analyzed *in situ* during indentation using the Raman spectroscopy-enhanced instrumented indentation technique (RSE-IIT), which has been described in detail in previous publications [16–19]. The tested Si thin film was epitaxially grown in the (100) orientation (film thickness: 600 nm ± 60 nm) on a sapphire r-plane wafer (wafer thickness: 530 μm ± 50 μm; uncertainties represent manufacturer specifications). In a first Raman experiment (mapping experiment), images of the contact region between sample and probe were collected *in situ* during hold periods of individual indentations, in which a force was applied to the probe, held constant for the duration of mapping and then released. The (un)loading rates were set to 5 mN/s. Images were collected for a peak indentation force of 50 mN. Twenty individual spectra were collected at evenly spaced locations along 15 μm scan ranges in two orthogonal directions, generating a 20 × 20 hyperspectral dataset

* Corresponding author at: *Material Measurement Laboratory, National Institute of Standards and Technology, Gaithersburg, MD 20899, USA.*
E-mail address: yvonne.gerbig@nist.gov (Y.B. Gerbig).

http://dx.doi.org/10.1016/j.scriptamat.2016.04.007
1359-6462/

(image). The collection time for an individual Raman spectrum was set to 15 s. A qualitative assessment of the Raman images suggested a lateral resolution of approximately 1 μm. In a second experiment (hold experiment), an indentation at 50 mN was held for an hour-long period, in which individual Raman spectra were collected every 10 s at the same location inside the contact region. In a third experiment (load-unload experiment), the Berkovich probe was loaded to a maximum force of 50 mN and then completely unloaded (no hold period, load and unload rates of 1.5 mN/s). A Raman spectrum was measured at the same location within the contact region approximately every 3 s, beginning 25 s prior to and continuing for 25 s after the completion of the indentation. The collection time of an individual spectrum was limited to 3 s to enable the collection of multiple spectra during indentation while maintaining a reasonable signal-to-noise ratio. The nominal illumination power of the 785-nm light source was set to 5 mW at the sample surface. The Raman spectra were fit to a model spectrum (200 cm^{-1} to 700 cm^{-1}) consisting of a series of bands of Pearson VII lineshape using a conventional non-linear least squares algorithm implemented in a custom spectroscopic image analysis program written in IDL (Exelis; McLean, VA) [20].

To illustrate the indentation-induced structural changes in Si and their corresponding spectral signatures, individual Raman spectra collected (a) prior to testing and (b) under an indentation force of 50 mN in the Raman mapping experiment are shown in Fig. 1. The Raman spectrum taken prior to testing (Fig. 1a) features peaks located at 378 cm^{-1} and 418 cm^{-1}, both associated with the sapphire substrate (labeled S1and S2) [18–19], and at 520 cm^{-1} and 290 cm^{-1}, attributed to the longitudinal optical mode (LO) and second-order transverse acoustic (2TA) mode of dc-Si [21], respectively. Significant spectral changes were observed under loading (Fig. 1b): Three broad Raman bands appeared and were assigned to the transverse optical (TO-a), longitudinal acoustic (LA-a), and LO (LO-a) modes of amorphous Si (a-Si) [22]. The occurrence of these bands indicates amorphization due to defects induced by the severe deformation under the acute indenter probe [14]. At the same time, a shoulder (LO-dc2) emerged on the high wavenumber side of the LO peak of dc-Si, believed to be due to elastic deformation of the dc-lattice surrounding the severely plastically deformed material [18]. Furthermore, several narrow peaks, P1 to P4, were observed. This grouping of peaks is similar to the spectral profile of bc8 and r8 [23–26] rather than β-tin (or Imma, sh) [27] observed during compression in DAC tests [1] and postulated to form on indentation loading [3,28]. To verify that the r8 and bc8 modes originate from the center of the contact and not from extruded and phase transformed material at the contact periphery [29,30], the spatial distribution of these modes in the contact region was visualized by mapping the intensity of the strongest peak (P1). Fig. 1(c) is an overlay of a grayscale plot of the intensity of that peak and a colored contour plot of the relative Raman shift of the LO-dc2 peak. As negative Raman shifts are associated with tensile strain and positive shifts with compressive strain [31], the compressed contact region can easily be identified in the contour map. The highest intensity (concentration) of peak P1 is indeed found in the center of the contact, indicating that the r8 and bc8 modes did not derive from extruded material.

Fig. 2 illustrates the temporal evolution of the spectral profile recorded during the hold experiment for a fixed location inside the contact region. Note that an additional peak, labeled P5, was observed in this experiment. The best-fit lines for P5 and P1 are shown as orange and green lines, respectively. To facilitate the identification of individual Raman features, Fig. 2 also summarizes theoretical values [24,32] and experimentally determined ranges [23,25,32–35] for the peak positions of r8, bc8, and β-tin modes observable in the spectral region covered by this study. Based on the literature data, peaks P1 and P4 can be assigned

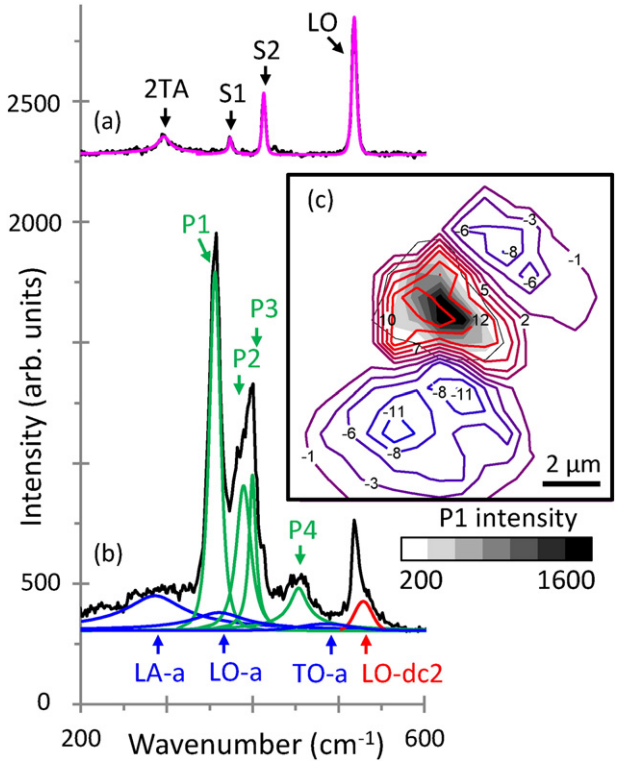

Fig. 1. Mapping experiment: Individual Raman spectra collected (a) prior to testing and (b) under an indentation load of 50 mN. In these spectra, the black curves are experimental data and the colored curves show fitted data for the various peaks. (c) Overlay of two images of the contact region collected at 50 mN: The colored contour plot shows the relative shift (cm^{-1}) of the center peak position of the LO-dc2 mode. The grayscale plot shows the spatial distribution of P1 by plotting its intensity. A Raman shift of the LO-dc2 mode towards smaller wavenumbers (blue) is associated with tensile strain and a shift towards larger wavenumbers (red) with compressive strain.

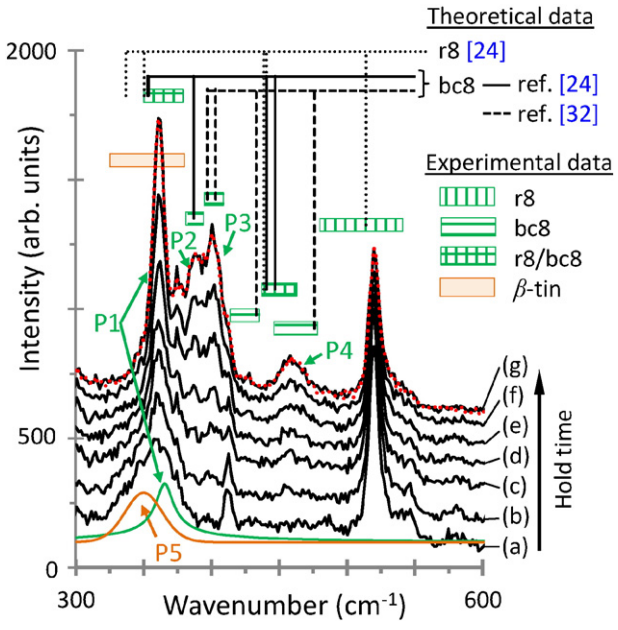

Fig. 2. Hold experiment: Evolution of the spectral features at a fixed location within the contact region under constant load for different hold times (a) 8 min, (b) 9 min, (c) 9.5 min, (d) 10 min, (e) 11 min, (f) 14 min, and (g) 36 min and 60 min (dotted line). Graph (a) represents the spectral profile observed from the start to 8 min into the hold period. The colored areas indicate the regions where Raman modes were observed for HPP modes in DAC tests [23,25,32,33] and β-tin mode in theoretical [34] and experimental [35] studies. The vertical lines indicate the theoretical peak frequency calculated for HPP modes [24,32].

to either r8 or bc8, whereas P2 and P3 appear to be solely related to bc8. Peak P5 is located in a spectral region where both β-tin and r8 may have Raman modes. The existence of the r8 mode predicted in this range, however, has never been experimentally verified and hence an association of P5 with the experimentally documented β-tin mode seems more likely. As can be observed (Fig. 2a), peaks P1 and P5 were recorded immediately at the start of the hold period suggesting that the transition to the associated phases started during loading. With time, the intensity of P1 increased at the expense of P5 (Fig. 2a to g) and other peaks P2 to P4 emerged in the spectrum (from Fig. 2c onwards) implying a continuous formation of bc8, and perhaps r8 (no clear evidence of peaks that could solely be attributed to the formation of r8 was observed). Eventually, no further major changes in spectral profile were observed (from Fig. 2f onwards), as, presumably, the structural transition of all of the "transformation-eligible" material in the contact region was completed.

Fig. 3(a) shows the collection points (circles) for Raman spectra in relation to the indentation conducted in the load-unload experiment. Fig. 3(b) depicts the wavenumber and intensity of peaks P1 and P5 associated with bc8 and r8, hereafter referred to as high-pressure phases (HPP), and the β-tin phase. Changes in these spectral parameters due to the changing loading conditions in the analyzed location of the contact region are shown for both peaks. As suggested earlier, Fig. 3 confirmed the phase transition to β-tin and HPP during the loading segment of the indentation. The mode intensities of HPP increased with further progression of the indentation as a growing portion of the deformed material transformed to those crystallographic structures. The transformation appeared to accelerate (steepening of slope) at one point during unloading, coinciding with a discontinuity in the indentation force–displacement response (Fig. 3a). This observation seems to be in agreement with the previous findings that the rapid transition of

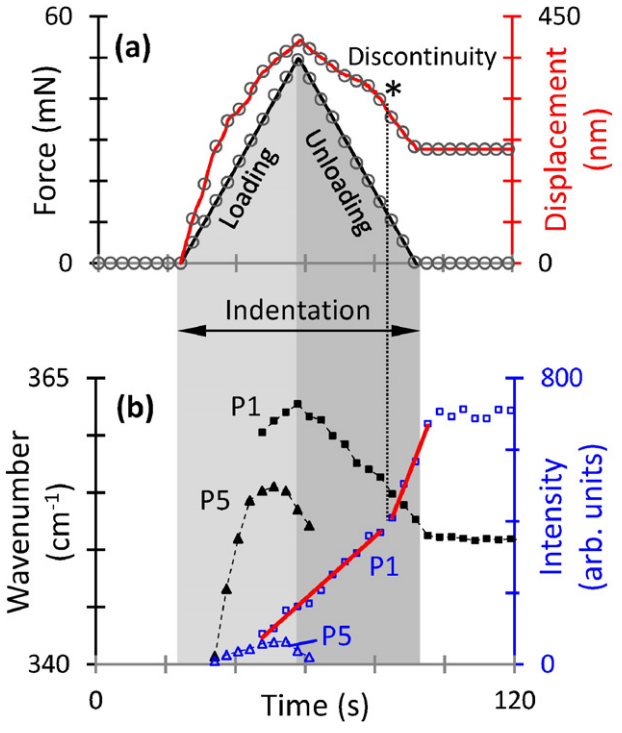

Fig. 3. Load–unload experiment: (a) The black curve shows the force applied to the sample and the red curves the displacement of the probe during indentation. The circles indicate the collection points of Raman spectra prior to, during, and after the indentation in the same location of the contact region. The asterisk marks a discontinuity observed in the indentation data. (b) Changes in wavenumber (filled symbols) and intensity (open symbols) for the spectral features P1 and P5 associated with HPP and β-tin. Wavenumber and intensity were determined from best-line fits for P1 and P5 similar to fits shown in Fig. 2. The red trend lines indicate the slope of the temporal intensity changes for P1. The dotted lines are a guide to the eye.

a substantial portion of material in the contact zone to the lower-density HPP causes a discontinuity (pop-out) in the force–displacement data [36]. A similar assessment of the displacement data collected in the second experiment (hold experiment) was not reliably possible, as displacement measurements were more strongly affected by drift effects during the longer test periods. The HPP mode position shifted continuously to higher wavenumbers during loading and reversed continuously to lower values during unloading (Fig. 3b) in accordance with its previously reported pressure dependence [23,25]. After full unloading, no further changes in intensity or peak position were observed.

In the literature, different scenarios for the transition path to HPP have been suggested: directly from dc [4,37,38], via lonsdaleite [5], or β-tin phases [24]. The data reported here seem to support the latter mechanism. The formation of HPP was first observed during decompression in DAC studies [24]. Consequently, it was inferred that decreasing pressure was a precondition for this transition. Based on those findings, it was assumed that the HPP formation could only occur in the unloading segment of indentations [3,11,36]. The validity of this assumption is challenged by observations in this study. Earlier works on the shear deformation of Si linked the formation of bc8 to the exposure to shear [4,5]. Therefore, it is suggested, that (shear) strain, in combination with hydrostatic pressure, needs to be considered in any future investigations into indentation-induced phase transformations. Also, a model has been proposed stating that HPP seeds nucleate within β-tin during unloading and eventually grow rapidly due to the increased instability of β-tin below a critical pressure in indentations [36]. In light of the new data reported here it appears prudent to revise the model to include strain as a trigger for nucleation and growth of HPP. It has been reported that the transition to HPP requires only relatively small strains (~2%) [24], which are easily achieved in indentations, especially with acute probes [39].

Furthermore, the observations of this study may provide context and insights into two other recently reported indentation-induced transformation phenomena. One study reported an increase in the portion of HPP found in residual indents after longer indentation holding periods with saturation being reached for holding periods longer than one hour [40]. As observed in the hold experiment (Fig. 2), nucleation and growth of HPP seem to be time-dependent. Once the nucleation is started, the transformation of all the transformation-eligible material in the deformation zone requires a certain growth time. Hence, larger portions of material transform to HPP with longer holding periods, as more time for nucleation and growth of HPP is available. However, as the amount of transformable material is restricted, an extension of the holding period beyond the growth time has no further effect. The time dependence of the HPP transition might also be reflected in another recent study: in cyclic indentations, an increased probability of pop-out events was observed for overall longer test durations, with pop-outs occasionally occurring during loading and holding periods [15]. Once initiated, the HPP transition progresses relatively slowly, and thus requires time to be completed. Pop-out events can be linked to the rapid growth of the HPP portion in the contact region (which seems to mark the end stage of HPP transitions). Hence, the more time that is given for the HPP transition to progress (the longer the test duration), the higher the probability of the completion of the HPP transition (manifested in pop-out events). Once the rapid growth is completed, a pop-out event can apparently occur under any loading condition (loading, holding, unloading, reloading segment) in the indentation test.

It should be noted that this study was conducted on thin Si films, rather than bulk Si as in the indentation studies cited. As stress levels and stress distribution are probably altered due to the different sample configuration, questions might be raised regarding the comparability of the presented data to those for bulk indentations. Some observations (e.g., regarding the sluggishness of the HPP transition) made in this study are similar to and confirm results reported for bulk indentations indicating a certain transferability of results. Nonetheless, although

more comprehensive study is certainly needed to describe the effect of strain and time on the HPP transition in more detail, the current study is important in reporting an observed deviation from the commonly assumed transformation sequence and pointing out a possible alternative to the accepted theory.

In summary, the indentation-induced phase transformation of crystalline Si thin films was studied *in situ* under an acute probe in different test regimes using RSE-IIT. *In situ* Raman spectroscopic analysis showed the formation of HPP during indentation loading, calling into question the common view that pressure release is a pre-condition for this transformation. The observations suggested strain and time as important but overlooked factors in nucleation and growth of HPP and provided new context to previous work on the pressure induced phase transformations of Si.

References

[1] A. Mujica, A. Rubio, A. Munoz, R.J. Needs, Rev. Mod. Phys. 75 (2003) 863.
[2] Y.G. Gogotsi, A. Kailer, K.G. Nickel, Mater. Res. Innov. 1 (1997) 3.
[3] V. Domnich, Y. Gogotsi, Rev. Adv. Mater. Sci. 3 (2002) 1.
[4] M.M. Aleksandrova, V.D. Blank, S.G. Buga, Phys. Solid State 35 (1993) 663.
[5] V.D. Blank, B.A. Kulnitskiy, High Pressure Res. 15 (1996) 31.
[6] J.J. Gilman, Philos. Mag. B 67 (1993) 207.
[7] M. Durandurdu, J. Phys. Condens. Matter 20 (2008) 325232.
[8] I.V. Gridneva, Y.V. Milman, V.I. Treflov, Phys. Status Solidi A 14 (1972) 177.
[9] D.R. Clarke, M.C. Kroll, P.D.J. Kirchner, R.F. Cook, B.J. Hockey, Phys. Rev. Lett. 60 (1988) 2156.
[10] G.M. Pharr, W.C. Oliver, R.F. Cook, P.D. Kirchner, M.C. Kroll, T.R. Dinger, D.R. Clarke, J. Mater. Res. 7 (1992) 96.
[11] S. Ruffell, J.E. Bradby, J.S. Williams, O.L. Warren, J. Mater. Res. 22 (2007) 578.
[12] C.F. Sanz-Navarro, S.D. Kenny, R. Smith, Nanotechnology 15 (2004) 692.
[13] C.R. Das, S. Dhara, Y.-R. Jeng, P.-C. Tsai, H.C. Hsu, B. Raj, A.K. Bhaduri, S.K. Albert, A.K. Tyagi, L.C. Chen, K.H. Chen, Appl. Phys. Lett. 96 (2010) 253113.
[14] Y.Q. Wu, Y.B. Xu, J. Mater. Res. 14 (1999) 682.
[15] H. Huang, J. Yan, Scr. Mater. 102 (2015) 35.
[16] Y.B. Gerbig, C.A. Michaels, A.M. Forster, J.W. Hettenhouser, W.E. Byrd, D.J. Morris, R.F. Cook, Rev. Sci. Instrum. 83 (2012) 125106.
[17] Y.B. Gerbig, C.A. Michaels, A.M. Forster, R.F. Cook, Phys. Rev. B 85 (2012) 104102.
[18] Y.B. Gerbig, C.A. Michaels, R.F. Cook, J. Mater. Res. 30 (2015) 390.
[19] Y.B. Gerbig, C.A. Michaels, J.E. Bradby, B. Haberl, R.F. Cook, Phys. Rev. B 92 (2015) 214110.
[20] Any mention of commercial products within this paper is for information only; it does not imply recommendation or endorsement by NIST.
[21] B.A. Weinstein, G.J. Piermarini, Phys. Rev. B 12 (1972) 1172.
[22] K. Winer, Phys. Rev. B 35 (1987) 2366.
[23] M. Hanfland, K. Syassen, High Pressure Res. 3 (1990) 242.
[24] R.O. Piltz, J.R. Maclean, S.J. Clark, G.J. Ackland, P.D. Hatton, J. Crain, Phys. Rev. B 52 (1995) 4072.
[25] H. Olijnyk, A.P. Jephcoat, Phys. Status Solidi B 413 (1999) 413.
[26] Z. Zeng, Q. Zeng, W.L. Mao, S. Qu, J. Appl. Phys. 115 (2014) 103514.
[27] K. Gaál-Nagy, D. Strauch, Phys. Rev. B 73 (2006) 014117.
[28] T. Kiriyama, H. Harada, J. Yan, Semicond. Sci. Technol. 25 (2009) 025014.
[29] A.B. Mann, D. van Heerden, J.B. Pethica, P. Bowes, T.P. Weihs, Philos. Mag. A 82 (2002) 1921.
[30] Y. Gogotsi, T. Miletich, M. Gardner, M. Rosenberg, Rev. Sci. Instrum. 70 (1999) 4612.
[31] E. Anastassakis, E. Liarokapis, J. Appl. Phys. 62 (1987) 3346.
[32] R.J. Kobliska, S.A. Solin, M. Selders, R.K. Chang, R. Alben, M.F. Thorpe, D. Weaire, Phys. Rev. Lett. 29 (1972) 725.
[33] G. Weill, J.L. Mansot, G. Sagon, C. Carlone, J.M. Besson, Semicond. Sci. Technol. 4 (1989) 280.
[34] H. Olijnyk, Phys. Rev. Lett. 68 (1992) 2232.
[35] K. Gaál-Nagy, M. Schmitt, P. Pavone, D. Strauch, Comput. Mater. Sci. 22 (2001) 49.
[36] S. Ruffell, J.E. Bradby, J.S. Williams, P. Munroe, J. Appl. Phys. 102 (2007) 063521.
[37] D.E. Kim, S.I. Oh, Nanotechnology 17 (2006) 2259–2265.
[38] H. Katzke, P. Toledano, J. Phys. Condens. Matter 19 (2007) 275204.
[39] Y.B. Gerbig, S.J. Stranick, R.F. Cook, Phys. Rev. B 83 (2011) 205209.
[40] O. Shikimaka, A. Priscaru, L. Bruk, Y. Usatyi, A. Burlacu, Surf. Eng. Appl. Electrochem. 48 (2012) 444.